Subwavelength Position Sensing Using Nonlinear Feedback and Wave Chaos

Seth D. Cohen, Hugo L. D. de S. Cavalcante, and Daniel J. Gauthier
Department of Physics, Duke University, Durham, North Carolina 27708, USA
(Received 16 August 2011; published 16 December 2011)

We demonstrate a position-sensing technique that relies on the inherent sensitivity of chaos, where we illuminate a subwavelength object with a complex structured radio-frequency field generated using wave chaos and nonlinear feedback. We operate the system in a quasiperiodic state and analyze changes in the frequency content of the scalar voltage signal in the feedback loop. This allows us to extract the object's position with a one-dimensional resolution of $\sim\lambda/10\,000$ and a two-dimensional resolution of $\sim\lambda/300$, where λ is the shortest wavelength of the illuminating source.

DOI: 10.1103/PhysRevLett.107.254103 PACS numbers: 05.45.Gg, 05.45.Mt, 84.30.Ng

Diffraction, a property of electromagnetic (EM) waves, blurs spatial information less than the wavelength λ of an illuminating source and hence limits the resolution of images. Over the past decade, techniques have been developed that overcome this diffraction limit using superlenses made from negative-index media [1,2], superoscillations [3], and nanostructures with surface plasmons [4,5]. Other methods use fluorescent molecules that serve as subwavelength point markers [6–9], where imaging is enabled by sensing the position of the markers.

In this Letter, we describe a new super-resolution technique that senses the position of an object by combining two concepts: nonlinear delayed feedback and wave chaos. The system uses radio frequency (rf) EM waves in a closed feedback loop through a wave-chaotic cavity. Self-oscillation in the feedback occurs when the loop gain exceeds the loop losses; no rf field is supplied by an external source. We include a nonlinear element (NLE) in the feedback loop to create complex (nonperiodic) dynamics with multiple independently stable frequencies. The resulting EM oscillations provide the illumination source for our position sensor.

Our work extends the Larsen effect, a phenomenon where positive audio feedback between a microphone and audio amplifier results in periodic acoustic oscillations. The frequency of oscillation, known as the Larsen frequency, is highly dependent on the propagation paths of the acoustic wave. A perturbation to these propagation paths shifts the Larsen frequency [10]. In addition, periodic oscillators with time-delayed feedback show extremely narrow and stable frequency spectra [11–14]. For our super-resolution position-sensing system, we exploit the sensitivity of quasiperiodic EM frequencies.

In our experimental system, the NLE is an input-output circuit based on the design from Ref. [15]. We use an aluminum two-dimensional (2D) quarter-stadium-shaped rf cavity as a well-known wave-chaotic scattering scene [16,17]. As shown in Fig. 1(a), the EM field emanating from the cavity is fed into a nonlinear circuit through a broadband (20 MHz–2 GHz) receiving (RX) antenna. The output of the circuit is fed back into the cavity through an identical transmitting (TX) antenna, creating a closed feedback loop. Inside the cavity is a subwavelength dielectric object.

The complex field inside of the cavity interacts multiple times with the object due to reflections from the cavity's walls [illustrated by a complex ray path in Fig. 1(a)] and from many passes of the rf signal through the nonlinear feedback loop. Because of these multiple interactions, small changes in the cavity alter the phase and amplitude of the field, affecting the spatial structure of the modes for a given frequency [10]. These changes alter the dynamical state of the system. The output of the nonlinear circuit is filtered such that its maximum frequency is 2 GHz, and thus the rf signal has $\lambda \geq 15$ cm.

The NLE in the EM feedback loop induces quasiperiodic oscillations with multiple incommensurate frequencies in the output voltage V_{out} of the nonlinear circuit. As the object moves inside the cavity, the frequencies of the quasiperiodic oscillations shift independently and provide a unique fingerprint of the object's location in 2D. Thus, we map the position of the object in both the x and y directions by monitoring changes of a single scalar voltage V_{out}.

Before describing our results, we first characterize our wave-chaotic cavity using its pulse response. Shown in Fig. 1(b), our cavity produces a complicated pulse response (typical of wave-chaotic systems) with a quality factor $Q = 174$ at a frequency of 1.77 GHz (the most prominent frequency in the quasiperiodic oscillations). As a result, broadcasting a continuous-wave signal into this cavity forms a complex interference pattern for each contained frequency. Generic cavities tend to display such wave chaos; only cavities with a high degree of symmetry display nonchaotic ray trajectories [18,19].

The pulse response of a wave-chaotic environment has been exploited to sense the appearance of an object in a scattering medium [20] or the location of a perturbation on the surface of a scattering medium [21]. These techniques rely on measuring changes to the pulse response and have demonstrated a spatial sensitivity of $\sim\lambda$. Our own work is

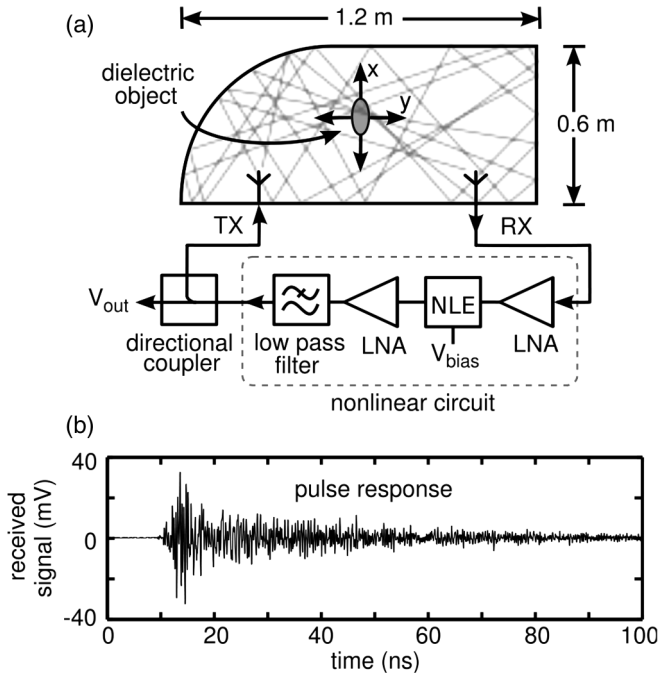

FIG. 1. (a) Experimental setup. Nonlinear circuit consisting of a transistor-based (BFG620) NLE, low-noise amplifiers (LNA, Mini-Circuits ZX60-4016E and Picosecond Pulse Labs 5828-108), and a low-pass filter. A bias voltage V_{bias} tunes the nonlinearity. The NLE is housed in a shielded aluminum box, but otherwise there is no active stabilization to control the thermal or vibrational effects of the environment. The output voltage V_{out} is measured with a 8-GHz-analog-bandwidth 40-GS/s oscilloscope (Agilent DSO80804B). Feedback passes through a cavity with a dielectric object (2 cm $\times$ 4 cm water-filled container) that is positioned in 2D using Thorlabs (LTS150) and Zaber Technologies (TLSR150B) translation stages. (b) Cavity pulse response. Here, the nonlinear circuit is removed to examine just the linear response of the cavity and antennas. We inject a 0.1 ns EM pulse of amplitude 1.5 V into the TX antenna and measure at the RX antenna. The time at which the radiation arrives at the RX antenna is a measure of the path length of EM energy through the cavity.

inspired by these achievements, where we use a continuous-time nonlinear feedback loop to achieve deep subwavelength position resolution.

Conventional oscillators using time-delayed nonlinear feedback use a nonlinear element whose output is amplified and coupled back to the input through a single feedback loop that delays the signal by a fixed amount. Because of the delayed feedback, these systems can display a variety of behaviors including periodic oscillations, quasiperiodicity, and chaos. Oscillators using time-delayed feedback have been designed using high-speed commercial electronics or lasers to generate complex signals with frequency bandwidths that stretch across several gigahertz [22–24].

Thus, the system shown in Fig. 1(a) combines the stability and sensitivity of a dynamical state from a high-speed nonlinear-feedback oscillator with the sensitivity and long propagation times of the EM field in a wave-chaotic cavity. The time delays of the feedback in this system are the propagation times for the EM energy to transmit through the cavity, rather than a single time delay.

The values of the delays and their respective gains form a continuous delay distribution (proportional to the cavity's pulse response) that is uniquely defined for each position of the enclosed object. This is known as a distributed-delay system, where the reflections of EM energy are the delay distribution. The pulse response in Fig. 1(b) demonstrates that the cavity stores EM energy for longer than 100 ns, where typical time scales of oscillations are less than 1 ns. As the time delay in feedback oscillators increases, the phase noise of oscillation frequencies decreases [12]. Thus, the system dynamics are stable for static configurations while also highly sensitive to changes in the cavity. Measuring the scalar variable V_{out}, we monitor dynamical changes in the system and sense the object's movements. We expect that this technique would be more or less general for all object positions in the cavity because of the ergodicity of ray trajectories.

We first demonstrate this idea qualitatively along a one-dimensional (1D) object path. We fix V_{bias} in the NLE to exhibit periodicity at $x = 0$ mm and measure the time evolution in V_{out} for object positions $x = 0$ mm–12 mm in 10 μm steps. The system changes between periodicity (P) from $x = 0$ mm–1.4 mm, quasiperiodicity (QP) from $x = 1.4$ mm–8 mm, and two different time-evolving chaotic states (C1 and C2) from $x = 8$ mm–9.8 mm and $x = 9.8$ mm–12 mm, respectively. Chaotic state C1 contains chaoticlike breathers and C2 exhibits a relatively flat bandwidth from 20 MHz—2 GHz.

The observed dynamical changes fall into one of two categories: an abrupt change in the dynamical state (known as a bifurcation) or small shifts in the frequency components and amplitudes of V_{out}. A bifurcation diagram illustrates the qualitative dynamical changes in Fig. 2. Our results show dynamical changes from subwavelength movements of a subwavelength object.

To go beyond the qualitative detection of movement, we tune V_{bias} so that V_{out} is in a quasiperiodic state (QP in Fig. 2) for all object positions of interest. The incommensurate frequencies of a QP state are not phase locked and hence can shift independently with respect to object translations. In addition, incommensurate frequencies help eliminate interference nodes (blind spots) of the illuminating EM waves in the cavity, where each frequency has a complex interference pattern that covers the blind spots of another. An example time series and frequency spectra for a fixed object position are seen in Figs. 3(a) and 3(b), respectively.

From Fig. 3, it is seen that the behavior of the voltage detected at the RX antenna is quasiperiodic, not chaotic in time. On the other hand, the shape of the cavity and the

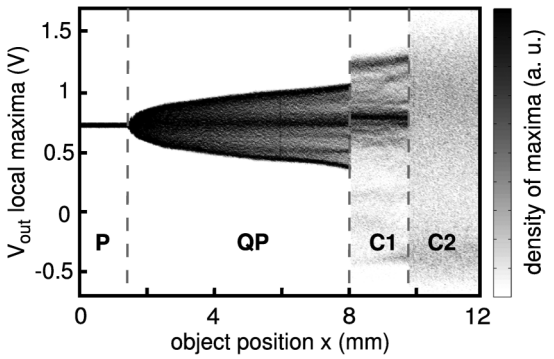

FIG. 2. Bifurcation Diagram. We store and analyze the time series of V_{out} at each object position along a 1D path in the x direction. The local maxima of each time series is plotted as a function of object position x.

presence of internal scatterers (object and antennas) create a complex EM field known as spatial wave chaos, even though the temporal behavior is quasiperiodic. The paths of rays in the cavity are highly sensitive to small changes, a hallmark of ray chaos, and this sensitivity in turn impacts the temporal dynamics of the oscillator.

Tracking the object entails measuring shifts in the QP frequency components. In Fig. 3(b), we highlight two peaks in the spectrum at frequencies denoted by f_1 and f_2. The frequency harmonics at $(f_2 - f_1)$ and $(f_2 + f_1)$ are used to improve the signal-to-noise ratio (SNR) of these frequencies. Averaging independent measures of f_1 and f_2 reduces statistical errors and increases their SNR. To follow changes in the frequencies of V_{out} with high precision, we use a nonlinear least-squares-fit to a model for a four-tone QP signal [11], resulting in a 2.4 kHz frequency resolution (approximately 0.5% of the total observed experimental frequency shifts).

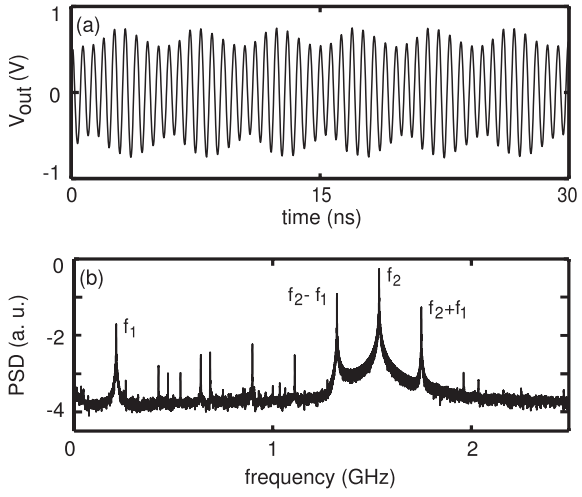

FIG. 3. (a) Temporal evolution of a typical quasiperiodic state used for position sensing. (b) Logarithmic power spectral density (PSD) of this signal.

To demonstrate 1D position sensing, we translate the object along the path $x = 0$ mm–5 mm while $y = 2.5$ mm. We then translate the object along an orthogonal path $y = 0$–5 mm while $x = 2.5$ mm. Shown in Figs. 4(a) and 4(b), the measured frequency shifts Δf_1 and Δf_2 are plotted for 1D paths along the orthogonal x and y directions, respectively. We separately fit Δf_1 and Δf_2 in the x and y directions with second order polynomials

$$a_1\Delta f_1(x) + a_2\Delta f_2(x) = c_0 + c_1 x + c_2 x^2, \quad (1)$$

$$b_1\Delta f_1(y) + b_2\Delta f_2(y) = d_0 + d_1 y + d_2 y^2. \quad (2)$$

We optimize the coefficients a_i and c_i (b_i and d_i) using a nonlinear least-squares-fit to a model for the object position. The root-mean-square (rms) error for the frequency shift map is 1.45 kHz (0.86 kHz) along x (y). By inverting these maps, we calculate the measured object positions. The rms error between the actual and measured positions is 9.2 μm (23.7 μm) for x (y), which demonstrates a

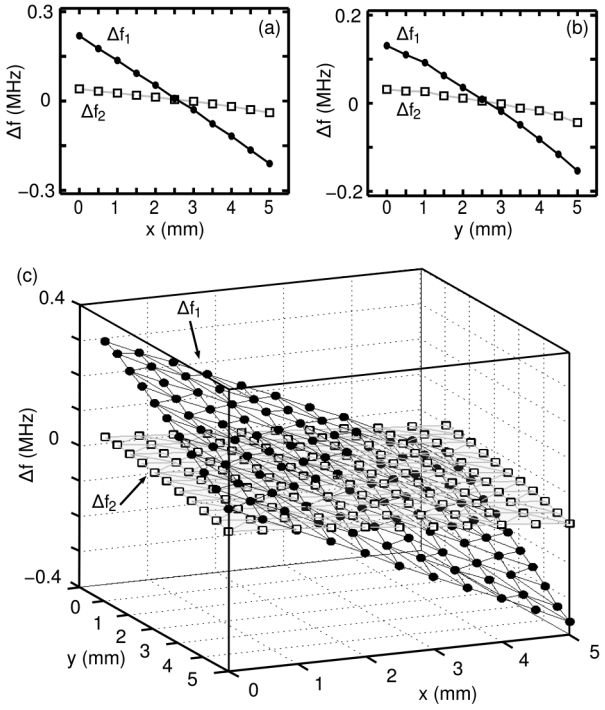

FIG. 4. Frequency shifts Δf_1 and Δf_2 of the QP state as the object translates along the (a) x direction, where the fit from Eq. (1) yields $a_1 = 2.8$ mm/kHz, $a_2 = -8.7$ mm/kHz, $c_0 = 27,113.0$ mm, $c_1 = -439.2$ and $c_2 = 1.5$ mm^{-1}, and (b) along the y direction, where the fit from Eq. (2) yields $b_1 = 0.8$ mm/kHz, $b_2 = -0.5$ mm/kHz, $d_0 = -73\,452.0$ mm, $d_1 = 242.0$, and $d_2 = -2.0$ mm^{-1}. (c) Frequency shifts $\Delta f_1(x, y)$ and $\Delta f_2(x, y)$ for object translations (x, y) in a 5 mm $\times$ 5 mm grid of positions. The planar fits from Eqs. (3) and (4) yield $\alpha_1 = -84.68$ kHz/mm, $\alpha_2 = -15.20$ kHz/mm, $\beta_1 = -56.74$ kHz/mm, $\beta_2 = -14.75$ kHz/mm, $\epsilon_1 = 11.72$ MHz and $\epsilon_2 = 2.43$ MHz. The measured determinant $|\alpha_1\beta_2 - \alpha_2\beta_1| = 386$ kHz^2/mm^2 with an error of 5.8 kHz^2/mm^2.

resolution of $\sim\lambda/10\,000$ along orthogonal 1D directions (recall $\lambda \geq 15$ cm).

Tracking the object's position in both the x and y directions simultaneously requires two independently changing observables. In our system, we observe a single scalar variable V_{out} that oscillates with primary frequencies f_1 and f_2. We fit the frequency shifts $\Delta f_1(x, y)$ and $\Delta f_2(x, y)$ for object positions (x, y) in a 5 mm $\times$ 5 mm area [Fig. 4(c)] and approximate them as planes

$$\Delta f_1(x, y) = \alpha_1 x + \beta_1 y + \epsilon_1, \tag{3}$$

$$\Delta f_2(x, y) = \alpha_2 x + \beta_2 y + \epsilon_2. \tag{4}$$

Using Cramer's rule, we show that $|\alpha_1\beta_2 - \alpha_2\beta_1| \neq 0$ to verify the planes are linearly independent in this area and allow us to simultaneously measure x and y coordinates.

In the 1D case, we have the freedom to optimize the fitting parameters in Eqs. (1) and (2) for x and y separately. In the 2D case, all of the fitting parameters α_i, β_i, and ϵ_i in Eqs. (3) and (4) are present in the solutions for both x and y. Thus, we cannot optimize the fits in the x and y directions separately and instead use the fitted planes for our frequency maps.

This constraint, combined with the approximation that these surfaces are planar, limits our 2D resolution. A planar fit of $\Delta f_1(x, y)$ ($\Delta f_2(x, y)$) gives a rms frequency error of 4.17 kHz (7.26 kHz) and a rms position error of 370 μm (650 μm) for x (y), yielding a 2D resolution of $\sim\lambda/300$. Higher order fits do not improve the resolution due to noise in our measurements. This 2D frequency mapping serves as the calibration for objects of this shape and must be reacquired for different shaped objects.

For comparison, a scanning near-field microwave microscope uses rf frequency shifts to achieve subwavelength sensitivity ($\sim \lambda/750\,000$) of near planar surfaces [25]. In contrast, our system uses nonlinear feedback to internally generate multiple independent frequencies and measures multiple degrees of freedom using a single scalar variable. Moreover, it uses a stationary pair of antennas to extract 2D spatial information of a 3D object, making it free of mechanically moving parts.

We conjecture that our method can be implemented using EM waves in the visible part of the spectrum. Semiconductor lasers with time-delayed optical feedback are known to display complex dynamical behaviors in which the output intensity varies in time, including quasiperiodicity [26–28]. Furthermore, optical wave chaos has been demonstrated using optical cavities [19,29,30]. We envision a completely optical version of our technique where a laser receives feedback from a wave-chaotic optical cavity. Such a system will be capable of tracking an object on a subnanometer scale.

Understanding the full potential of this method will require studies in both wave chaos and nonlinear dynamics. Our results suggest that one can position sense in 3D using a QP state with three independent frequencies. This type of dynamical state is possible in our system but requires further study to create a QP state for a 3D volume of interest. More independent observables could also be introduced into the system using two or more feedback loops external to the cavity, where each loop is independently band limited to prevent cross talk.

In the future, we see several options to improve the system's resolution. Currently, resolution limitations are based on the SNR of V_{out} as well as the long-term drift of the system. Increasing the number of frequency harmonics through nonlinear mixing gives additional measures of the independent modes and improves the system's SNR. Also, the cavity Q is proportional to the number of interactions between the subwavelength object and the EM energy inside of the cavity, and thus the resolution of this technique should scale with Q. We are exploring methods to generalize our technique to multiple objects.

We believe that our system will have applications beyond just position sensing. For example, the scattering and absorption of a subwavelength object strongly depend on its geometry and surroundings, and our approach, which is sensitive to the shape and orientation of the scatterer, can quantitatively track these properties. Also, similar to [10], analyzing dynamical states can monitor changes in the EM properties of materials in the cavity.

To the best of our knowledge, our approach is the first to measure multiple spatial degrees of freedom on a subwavelength scale using a single scalar signal. Using a QP analog of the Larsen effect, we combine a nonlinear feedback oscillator with multiple EM reflections in a scattering environment to exploit the inherent sensitivity of wave chaos, adding an alternative to the short list of superresolution techniques.

We gratefully acknowledge Zheng Gao with help in designing the NLE and the financial support of the U.S. Office of Naval Research Grant No. N000014-07-0734.

[1] X. Zhang and L. Zhaowei, Nature Mater. **7**, 435 (2008).
[2] J. Zhu, J. Christensen, J. Jung, L. Martin-Moreno, X. Yin, L. Fok, X. Zhang, and F. J. Garcia-Vidal, Nature Phys. **7**, 52 (2010).
[3] F. M. Huang, C. Yifang, F. J. G. Abajo, and N. I. J. Zheludev, J. Opt. A **9**, S285 (2007).
[4] W. L. Barnes, A. Dereux, and T. W. Ebbesen, Nature (London) **424**, 824 (2003).
[5] J. N. Anker, W. P. Hall, O. Lyandres, N. C. Shah, J. Zhao, and R. P. V. Duyneand, Nature Mater. **7**, 442 (2008).
[6] E. Rittweger, K. Y. Han, S. E. Irvine, C. Eggeling, and S. W. Hell, Nature Photon. **3**, 144 (2009).
[7] X. Zhuang, Nature Photon. **3**, 365 (2009).
[8] M. G. L. Gustafsson, Proc. Natl. Acad. Sci. U.S.A. **102**, 13 081 (2005).

[9] R. Heintzmann and M. G. L. Gustafsson, Nature Photon. **3**, 362 (2009).
[10] O. I. Lobkis and R. L. Weaver, J. Acoust. Soc. Am. **125**, 1894 (2009).
[11] R. L. Weaver and O. I. Lobkis, J. Acoust. Soc. Am. **120**, 102 (2006).
[12] X. S. Yao and L. Maleki, J. Opt. Soc. Am. B **13**, 1725 (1996).
[13] J. Lasri, P. Devgan, R. Tang, and P. Kumar, IEEE Photonics Technol. Lett. **16**, 263 (2004).
[14] Y. K. Chembo, L. Larger, and P. Colet, IEEE J. Quantum Electron. **44**, 858 (2008).
[15] L. Illing and D. J. Gauthier, Chaos **16**, 033119 (2006).
[16] H. Alt, H. D. Gräf, H. L. Harney, R. Hofferbert, H. Lengeler, A. Richter, P. Schardt, and H. A. Weidenmüller, Phys. Rev. Lett. **74**, 62 (1995).
[17] H. J. Stöckmann and J. Stein, Phys. Rev. Lett. **64**, 2215 (1990).
[18] J. U. Nöckel, A. D. Stone, and R. K. Chang, Opt. Lett. **19**, 1693 (1994).
[19] J. U. Nöckel and A. D. Stone, Nature (London) **385**, 45 (1997).
[20] B. Taddese, J. T. Hart, T. M. Antonsen, E. Ott, and S. M. Anlage, J. Appl. Phys. **108**, 114911 (2010).
[21] R. K. Ing and N. Quieffin, Appl. Phys. Lett. **87**, 204104 (2005).
[22] Y. C. Kouomou, P. Colet, L. Larger, and N. Gastaud, Phys. Rev. Lett. **95**, 203903 (2005).
[23] R. Zhang, H. L. De S. Cavalcante, Z. Gao, D. J. Gauthier, J. E. S. Socolar, M. M. Adams, and D. P. Lathrop, Phys. Rev. E **80**, 045202(R) (2009).
[24] T. E. Murphy, A. B. Cohen, B. Ravoori, K. R. B. Schmitt, A. V. Setty, F. Sorrentino, C. R. S. Williams, E. Ott, and R. Roy, Phil. Trans. R. Soc. A **368**, 343 (2009).
[25] M. Tabib-Azar, D.-P. Su, A. Pohar, S. R. LeClair, and G. Ponchak, Rev. Sci. Instrum. **70**, 1725 (1999).
[26] K. Ikeda, H. Daido, and O. Akimoto, Phys. Rev. Lett. **45**, 709 (1980).
[27] J. Mørk, J. Mark, and B. Tromborg, Phys. Rev. Lett. **65**, 1999 (1990).
[28] I. Fischer, O. Hess, W. Elsässer, and E. Göbel, Phys. Rev. Lett. **73**, 2188 (1994).
[29] C. Gmachl, F. Capasso, E. E. Narimanov, J. U. Nöckel, A. D. Stone, J. Faist, D. L. Sivco, and A. Y. Cho, Science **280**, 1556 (1998).
[30] T. Gensty, K. Becker, I. Fischer, W. Elsässer, C. Degen, P. Debernardi, and G. P. Bava, Phys. Rev. Lett. **94**, 233901 (2005).